https://doi.org/10.5194/bg-2020-57
Preprint. Discussion started: 9 March 2020

Biogeosciences Discussions
Open Access
EGU

Effects of ^{238}U variability and physical transport on water column ^{234}Th downward fluxes in the coastal upwelling system off Peru

Ruifang C. Xie[1]*, Frédéric A. C. Le Moigne[2], Insa Rapp[1], Jan Lüdke[1], Beat Gasser[3], Marcus Dengler[1], Volker Liebetrau[1], Eric P. Achterberg[1]

[1]GEOMAR Helmholtz Center for Ocean Research Kiel, Wischhofstrasse 1-3, 24148 Kiel, Germany

[2]Mediterranean Institute of Oceanography (UM 110, MIO), CNRS, IRD, Aix Marseille Université, Marseille, France

[3]IAEA Environment Laboratories, 4 Quai Antoine 1er, 98000 Monaco Monaco

* corresponding author: rxie@geomar.de

https://doi.org/10.5194/bg-2020-57
Preprint. Discussion started: 9 March 2020

Biogeosciences Discussions

Abstract

The eastern boundary region of the southeast Pacific Ocean hosts one of the world's most dynamic and productive upwelling systems with an associated oxygen minimum zone (OMZ). The variability in downward export fluxes in this region, with strongly varying surface productivity, upwelling intensities and water column oxygen content, is however poorly understood. Thorium-234 (^{234}Th) is a powerful tracer to study the dynamics of export fluxes of carbon and other elements, yet intense advection and diffusion in nearshore environments impact the assessment of depth-integrated ^{234}Th fluxes when not properly evaluated. Here we use ADCP current velocities, satellite wind stress and *in situ* microstructure measurements to determine the magnitude of advective and diffusive fluxes over the entire ^{234}Th flux budget at 25 stations from 11°S to 16°S in the Peruvian OMZ. Contrary to findings along the GEOTRACES P16 eastern section, our results showed that weak surface wind stress during our cruises induced low upwelling rates and minimal upwelling ^{234}Th fluxes, whereas vertical diffusive ^{234}Th fluxes were important only at a few shallow shelf stations. Similarly, horizontal advective and diffusive ^{234}Th fluxes were negligible due to small alongshore ^{234}Th gradients. Our data indicated a poor correlation between seawater ^{238}U activity and salinity. Assuming a linear relationship between the two would lead to significant underestimations of the total ^{234}Th flux by up to 40% in our study. Proper evaluation of both physical transport and variability in ^{238}U activity is thus crucial in coastal ^{234}Th flux studies. Finally, we showed large temporal variations on ^{234}Th residence times across the Peruvian upwelling zone, and cautioned future carbon export studies to take these temporal changes into consideration while evaluating carbon export efficiency.

Keywords: eastern tropical South Pacific, ^{234}Th tracer, uranium-salinity correlation, physical processes, residence time

https://doi.org/10.5194/bg-2020-57
Preprint. Discussion started: 9 March 2020


Biogeosciences Discussions Open Access EGU

1. Introduction

Isotopes of thorium (Th) are widely used as tracers for particle cycling in the oceans (Waples et al., 2006). In particular, ^{234}Th has been extensively used to trace particle dynamics and export fluxes, and to quantify the marine budgets of important macro- and micronutrients such as carbon (C), nitrogen (N), phosphorus (P) and iron (Fe) (Bhat et al., 1968;Buesseler et al., 1992;Coale and Bruland, 1987;Lee et al., 1998;Le Moigne et al., 2013;Cochran and Masqué, 2003;Van Der Loeff et al., 2006;Black et al., 2019). ^{234}Th has a relatively short half-life ($\tau_{1/2}$ = 24.1 days) that allows studies of biological and physical processes occurring on timescales of days to weeks. Unlike its radioactive parent uranium-238 (^{238}U, $\tau_{1/2}$ = 4.47 Ga) that is soluble in seawater, ^{234}Th is highly particle reactive and strongly scavenged by particles (Bhat et al., 1968). Generally, a deficit of ^{234}Th relative to ^{238}U is observed in the surface ocean and reflects net removal of ^{234}Th due to particle sinking, whereas secular equilibrium between ^{234}Th and ^{238}U is observed for intermediate and deep waters. Integrating this surface ^{234}Th deficit with depth yields the sinking flux of ^{234}Th and, if elemental:^{234}Th ratios are known, the sinking flux of elements such as C, N, P, and trace metals (Bhat et al., 1968;Buesseler et al., 1998;Buesseler et al., 1992;Coale and Bruland, 1987;Weinstein and Moran, 2005;Buesseler et al., 2006;Owens et al., 2015;Black et al., 2019).

Various ^{234}Th models have been put forward to study adsorption/desorption, aggregation and export, but single box models that assume negligible ^{234}Th fluxes due to physical transport are commonly used to calculate oceanic ^{234}Th-derived particle fluxes (see detailed review by Savoye et al., 2006). This assumption is typically appropriate in open ocean settings where ^{234}Th fluxes due to advection and diffusion are small relative to the downward fluxes of ^{234}Th associated with particle sinking. However, in upwelling regions such as the equatorial Pacific and

https://doi.org/10.5194/bg-2020-57
Preprint. Discussion started: 9 March 2020

coastal systems, advective and diffusive ^{234}Th fluxes may become increasingly important (e.g., Bacon et al., 1996;Buesseler et al., 1998;Buesseler et al., 1995;Dunne and Murray, 1999). For example, in the equatorial Pacific, strong upwelling post El-Niño could account for ~50% of the total ^{234}Th fluxes (Bacon et al., 1996;Buesseler et al., 1995). Ignoring the upwelling term could thus lead to an underestimation of ^{234}Th fluxes by a factor of 2. Conversely, horizontal diffusion carrying recently upwelled, ^{234}Th replete waters has been shown to balance the upwelled ^{234}Th fluxes in the central equatorial Pacific (Dunne and Murray, 1999). To the contrary, advective and diffusive ^{234}Th fluxes were minimal off the Crozet Islands in the Southern Ocean due to limited horizontal ^{234}Th gradients, long residence time of water masses, and low upwelling rates and diffusivities (Morris et al., 2007).

The dynamic nature of coastal processes requires that physical terms be included in ^{234}Th flux calculation whenever possible. Accurate measurements of current velocities and diffusivities are however challenging and thus direct observations of the effects of physical processes on ^{234}Th distributions in coastal regions are scarce. Limited studies have incorporated advection and diffusion in the nearshore zones of the Arabian Sea (Buesseler et al., 1998), Gulf of Maine (Gustafsson et al., 1998;Benitez-Nelson et al., 2000), the South China Sea (Cai et al., 2008) and Peruvian oxygen minimum zone (OMZ) (Black et al., 2018). In the Arabian Sea, coastal upwelling during a southwest monsoon could account for over 50% of the total ^{234}Th flux (Buesseler et al., 1998). Horizontal advection has been shown to be substantial in the Inner Cosco Bay of the Gulf of Maine (Gustafsson et al., 1998), whereas offshore advection and diffusion are only important in late summer (Benitez-Nelson et al., 2000). Therefore, the importance of physical processes on the ^{234}Th flux estimate is highly dependent on the seasonal and spatial variability of the current velocities, diffusivities and ^{234}Th gradients. In terms of the Peruvian OMZ, Black et al. (2018) showed that coastal upwelling accounts for >50% of total ^{234}Th fluxes

https://doi.org/10.5194/bg-2020-57
Preprint. Discussion started: 9 March 2020

at 12°S; however, how upwelling ^{234}Th fluxes varies seasonally and spatially in this region is unclear.

Another uncertainty in ^{234}Th flux calculations in such region stems from variations on dissolved ^{238}U activities. Generally speaking, U behaves conservatively under open ocean oxic conditions and is linearly correlated with salinity (Chen et al., 1986;Ku et al., 1977;Owens et al., 2011). However, numerous studies have shown that such correlation breaks down in various marine environments including the tropical Atlantic (Owens et al., 2011), Mediterranean Sea (Schmidt and Reyss, 1991), and Arabian Sea (Rengarajan et al., 2003). Although it is generally accepted that deviations from the linear ^{238}U-S correlation will lead to differences in the final calculated ^{234}Th fluxes, there is currently little knowledge on how significant these differences could be.

In this study, we report vertical profiles of ^{234}Th and ^{238}U along four transects perpendicular to the coastline of Peru (i.e. shore-normal transects). We evaluate the ^{238}U-S correlation in low-oxygen waters and how deviations from this correlation impact final ^{234}Th flux estimates. We also assess the spatial and temporal importance of advection and diffusion on ^{234}Th flux estimates.

2. Sampling and methods

2.1 Seawater sampling and analysis

Seawater samples were collected at 25 stations along 4 shore-normal transects between 11°S and 16°S in the Peruvian OMZ during two cruises M136 and M138 on board the RV Meteor (Figure 1). Cruise M136 took place in austral autumn (April 11 to May 3, 2017) along

https://doi.org/10.5194/bg-2020-57
Preprint. Discussion started: 9 March 2020

two main transects at 12°S and 14°S. Two stations from M136 (stations 458 and 495) were reoccupied within a week (repeat stations 508 and 516, respectively) to evaluate the steady-state assumption in the ^{234}Th flux calculation. The surface sample of the repeat station 508 was missing so only results from repeat stations 495 and 516 (occupation interval 1.5 days) were compared and discussed in terms of the non-steady state model (session 3.2). ^{234}Th sampling during cruise M138 was carried out in austral winter (June 1 to July 4, 2017) and focused on four shore-normal transects at 11°S, 12°S, 14°S and 16°S.

At each station, a stainless-steel rosette with Niskin bottles (Ocean Test Equipment®) was deployed for sampling of total ^{234}Th in unfiltered seawater and dissolved ^{238}U (0.2 µm pore size, Acropak® polycarbonate membrane). Each ^{238}U sample was acidified to pH ~1.6 at sea. High vertical resolution sampling was performed in the upper 200 m where most of the biological activity occurs; additional depths were sampled down to 600 m, or 50 m above the seafloor. Deep seawater at 1000 m, 1500 m, and 2000 m was sampled at three stations to determine the absolute β counting efficiency. Salinity, temperature, oxygen concentrations and fluorescence data (Table S1) were derived from the sensors (Seabird Electronics® 9plus system) mounted on the CTD frame (Krahmann, 2018;Lüdke et al., in review 2019).

Sample collection and subsequent chemical processing and analysis for total ^{234}Th followed protocols by Pike et al. (2005) and SCOR Working Group RiO5 cookbook (https://cmer.whoi.edu/). Briefly, a ^{230}Th yield tracer (1 dpm) was added to each sample before Th was extracted with MnO_2 precipitates. Precipitates were filtered onto 25 mm quartz microfiber filters (Whatman® QMA, 2.2 µm nominal pore size) and dried overnight at 50°C, after which they were counted at sea on a Risø® low-lever beta GM multicounter until uncertainty was below 3%, and again 6 months later at home laboratory for background ^{234}Th activities. After the second beta counting, filters were digested in an 8M HNO_3/10% H_2O_2 solution (Carl Roth®, trace metal

https://doi.org/10.5194/bg-2020-57
Preprint. Discussion started: 9 March 2020

131 grade). 10 dpm of ^{229}Th was added to each sample at the beginning of digestion to achieve a 1:1
132 atom ratio between ^{229}Th:^{230}Th. Digested samples were diluted in 2.5% HNO_3/0.01% HF mixture
133 and ^{229}Th/^{230}Th ratios were measured using an ICP-MS (ThermoFisher® Element XR) to
134 determine the chemistry yield and final ^{234}Th activities. The average yield was calculated to be
135 97% ± 6% (n = 247). For a subset of samples (marked in Table S1) whose analysis failed during
136 initial ICP-MS measurement, anion chromatography (Biorad® AG1x8, 100 – 200 mesh, Poly-
137 Prep columns) was performed to remove Mn from the sample matrix before another ICP-MS
138 analysis. This subset of samples also included three samples (marked in Table S1) whose initial
139 ICP-MS measurement was successful, to test whether anion chromatography affects final ICP-
140 MS results. Identical ^{229}Th/^{230}Th ratios were measured for samples with and without column
141 chromatography (see Table S1 footnotes for details).
142 Samples of dissolved ^{238}U were diluted 20 times in 1N HNO_3 at home laboratory and
143 spiked with an appropriate amount of ^{236}U spike to achieve ^{236}U:^{238}U ~ 1:1. Ratios of ^{236}U:^{238}U
144 were analyzed by ICP-MS (ThermoFisher Element XR) and activities of ^{238}U were calculated
145 using isotope dilution. Seawater certified reference materials (CRMs), CASS-6 and NASS-7, and
146 the International Association for the Physical Sciences of the Oceans (IAPSO) standard seawater
147 were analyzed routinely for uranium concentrations.

148

149 2.2 Flux calculation

150 Assuming a one box model, the temporal change of ^{234}Th activities is balanced by
151 production from ^{238}U, radioactive decay of ^{234}Th, removal of ^{234}Th onto sinking particles, and
152 transport into or out of the box by advection and diffusion (Bhat et al., 1968;Savoye et al., 2006;
153 and references therein):

https://doi.org/10.5194/bg-2020-57
Preprint. Discussion started: 9 March 2020

$$\frac{\partial A_{Th}}{\partial t} = \lambda(A_U - A_{Th}) - P + V \quad (1)$$

where A_U and A_{Th} are respectively the activities of dissolved ^{238}U and total ^{234}Th, λ is the decay constant of ^{234}Th, P is the net removal flux of ^{234}Th, and V is the sum of advective and diffusive fluxes. At times when repeat sampling is not possible within adequate cruise timeframe, steady state conditions are generally assumed, i.e. $\frac{\partial A_{Th}}{\partial t} = 0$. In this case, Eq. (1) is simplified into:

$$P = \int_0^z \lambda(A_U - A_{Th})dz + V \quad (2)$$

The vertical flux of ^{234}Th, P (dpm/m^2/d), is integrated to the depth of interest. Earlier studies generally used arbitrarily fixed depths (e.g., the base of mixed layer, or ML) for ^{234}Th and POC flux estimates (Bacon et al., 1996;Buesseler et al., 1992). Recent studies emphasized the need to normalize POC flux to the depth of euphotic zone (EZ), which separates the particle production layer in the surface from the flux attenuation layer below (Black et al., 2018;Buesseler and Boyd, 2009;Rosengard et al., 2015). In the open ocean, the depth of EZ is generally similar to ML depth. For the purpose of this study, the slight difference of the exact depth chosen (ML vs. EZ) was of little relevance to the significance of physical processes and ^{238}U variability.

2.3 Quantification of the physical fluxes

The physical term V in Eq. (2) is expressed as following:

$$V = \int_0^z \left(\omega \frac{\partial Th}{\partial z} - u\frac{\partial Th}{\partial x} - v\frac{\partial Th}{\partial y}\right) dz + \int_0^z \left(k_x \frac{\partial^2 Th}{\partial x^2} + k_y \frac{\partial^2 Th}{\partial y^2} - k_z \frac{\partial^2 Th}{\partial z^2}\right) dz \quad (3)$$

https://doi.org/10.5194/bg-2020-57
Preprint. Discussion started: 9 March 2020

where ω is the upwelling rate (m s^{-1}), u and v respectively the zonal and meridional current velocities, and k_x, k_y, and k_z diffusivities (m^2 s^{-1}) on the zonal, meridional and vertical directions, respectively.

Upwelling velocities at stations within 60 nautical miles of the coast, where upwelling is the most significant, were estimated from monthly wind stress following Steinfeldt et al. (2015). Daily wind stress from Metop/ASCAT scatterometer with a spatial resolution of 0.25° (Bentamy and Croize-Fillon, 2010) was obtained from the Centre de Recherche et d'Exploitation Satellitaire (CERSAT), at IFREMER, Plouzané (France). Zonal and meridional current velocities derived from vessel mount acoustic doppler current profiler (VmADCP) (Lüdke et al., in review 2019) were applied in Eq. (3) to assess horizontal advective fluxes. The top 30 m surface layer for M136 and top 50 m for M138 were considered; these depths correspond to 5-20 m below the base of the ML during each cruise. Zonal and meridional current velocities for each station were averaged over 5 days before and after station occupation. These current velocities were further averaged over a 10 km radian at stations closest to shore (St. 353, 428, 458, 475, 508, 904, and 907) and over a 50 km radian at the rest of the stations.

Average vertical diffusivity for both shallow (bottom depth < 500 m) and deep stations (bottom depth > 500 m) were calculated using *in situ* microstructure profiler measurements from cruises M136 (Thomsen and Lüdke, 2018) and M137 (unpublished data; May 6 – 29, 2017) (Figure S1), and stratification derived from CTD profiles following the methodology described in Fischer et al. (2013). *In situ* microstructure measurements during cruise M138 are not available but there were little variations amongst individual microstructure profiles during both M136 and M137 despite drastic change in the intensities of the poleward Peru Chile Undercurrent (Lüdke et

https://doi.org/10.5194/bg-2020-57
Preprint. Discussion started: 9 March 2020

al., in review 2019). It thus appears appropriate to apply this average vertical diffusivity to stations during M138.

Horizontal diffusivity, or eddy diffusivity, was not measured during the cruises. Surface eddy diffusivities in the North Atlantic OMZ were estimated to be on the order of a few 1000 m^2 s^{-1} that decrease exponentially with depth (Hahn et al., 2014). Similar magnitude of eddy diffusivities was estimated for the ETSP based on surface drifter data and satellite altimetry (Abernathey and Marshall, 2013;Zhurbas and Oh, 2004). We thus consider an eddy diffusivity of 1000 m^2 s^{-1} as a good approximate in this study for the evaluation of horizontal diffusive ^{234}Th fluxes. Applying this eddy diffusivity and horizontal ^{234}Th gradient in Eq. (3) would a yield maximum horizontal diffusive ^{234}Th flux of 10 dpm m^{-2} d^{-1} (see section 3.2 for how horizontal ^{234}Th gradient was calculated), which is insignificant (<1% of total ^{234}Th flux) at all stations. We thus ignore this horizontal diffusive term in the following discussion.

3. Results and discussion

The vertical profiles of ^{238}U and ^{234}Th activities are shown in Figure 2 and tabulated in Table S1. Data from station 508 were reported in Figure 2 and Table S1 but excluded in the following discussion, because the surface sample from this station was missing, which prevents any flux calculation. Also tabulated in Table S1 are temperature, salinity and concentrations of oxygen and fluorescence derived from the CTD sensors. Uranium concentrations of CRMs and the IAPSO standard seawater are reported in Table S2. Average U concentrations of both CASS-6 (2.77 ± 0.04 ng g^{-1}, 1SD, n = 5) and NASS-7 (2.86 ± 0.05 ng/g, 1SD, n = 5) measured in this study agree well with certified values (2.86 ± 0.42 ng g^{-1} and 2.81 ± 0.16 ng g^{-1}, respectively). Average ^{238}U concentrations measured in our IAPSO standard seawater (OSIL batch P156) (3.24

https://doi.org/10.5194/bg-2020-57
Preprint. Discussion started: 9 March 2020

± 0.06 ng g^{-1}, 1SD) is slightly higher than that reported in Owens et al. (2011) (3.11 ± 0.03 ng g^{-1}, 1SD, OSIL P149), and may reflect slight differences in U concentrations between different OSIL batches.

Activities of ^{238}U showed small to negligible variations (< 6% of the profile mean) with depth. All stations showed large ^{234}Th deficits in surface waters with $^{234}Th/^{238}U$ ratios as low as 0.25 (Figure 2). ^{234}Th at all stations generally reached equilibrium with ^{238}U at depths between 30 m and 250 m. At St. 912, deficits of ^{234}Th extended beyond 600 m depth. The equilibrium depths did not vary as a function of depths of either mixed layer or the upper oxic-anoxic interface, nor the magnitude of surface fluorescence concentrations (Table 1). The following stations (St. 428, 879, 898, 906, 907, 915, 919) displayed a secondary ^{234}Th deficit below the equilibrium depth, indicative of ^{234}Th removal processes. A small ^{234}Th excess at depth was only observed for St. 559.

In the following sections, we assessed the effects of seawater ^{238}U variability and physical transport on ^{234}Th flux estimates.

3.1 Lack of linear ^{238}U – salinity correlation in the Peruvian OMZ

Water column ^{238}U and salinity displayed poor linear correlation across the entire Peruvian OMZ regardless of seawater oxygen concentrations (Figure 3a-b). The general consensus is that U behaves conservatively in oxic seawater in the open ocean and early observations have shown that ^{238}U activities can be calculated from salinity based on a simple linear correlation between the two (e.g. Chen et al., 1986;Ku et al., 1977). Recent compilations in Van Der Loeff et al. (2006) and Owens et al. (2011) further demonstrated that the majority of

https://doi.org/10.5194/bg-2020-57
Preprint. Discussion started: 9 March 2020

uranium data points in the global seawater dataset follow a linear correlation with seawater salinity. The ^{238}U-salinity formulations from either Chen et al. (1986) or Owens et al. (2011) are thus generally appropriate for open ocean conditions and have been widely used in ^{234}Th flux studies. However, this linear ^{238}U-salinity correlation breaks down in the Peruvian OMZ.

Furthermore, the measured ^{238}U activities in this study correlated poorly with those calculated from salinity using the Owens formulation (Table S2, Figure 3c), with the former significantly higher than the projected values and differences up to 10%. This observation is in contrast to earlier studies in low oxygen waters where soluble U(VI) was reduced to insoluble U(IV) in suboxic/anoxic waters and removed from seawater (Rengarajan et al., 2003;Anderson et al., 1989). The consequence of this notable difference in ^{238}U to ^{234}Th flux according to Eq. (2) is neither linear nor straightforward, because the vertical gradients of both ^{238}U and ^{234}Th strongly affects the impacts of ^{238}U variations on ^{234}Th fluxes. In this study, ^{234}Th fluxes at 100 m derived from S-based ^{238}U lead to significant underestimation of ^{234}Th fluxes by an average of 20% and as high as 40% (Table 2). These differences in ^{234}Th fluxes will have direct consequences for ^{234}Th derived elemental fluxes such as C, N, P and trace metals.

Deviations from the linear ^{238}U-S correlation have been reported for shelf-estuary systems, where the behavior of dissolved U is highly variable with both removal and additions from sediments and settling particles (see detailed reviws in Cochran, 1992;Moore, 1992;Swarzenski et al., 2003). For example, Swarzenski et al. (2004) observed U removal on the Amazon shelf when salinity dropped below 12, whereas McKee et al. (1987) found significant U enrichment on the shelf at higher salinity (S > 10) that was attributed to remobilization of riverine sediments and subsequent desorption of U from ferric-oxyhydroxides. These findings agree with previous observations made during incubation experiments where sedimentary U was released to

https://doi.org/10.5194/bg-2020-57
Preprint. Discussion started: 9 March 2020

ambient fluid upon reduction of ferromanganese oxides (Barnes and Cochran, 1993). The Peruvian upwelling zone is not an estuary system nor directly influenced by major rivers. However, Fe reduction and release from the Peruvian shelf sediments (Noffke et al., 2012;Scholz et al., 2014) could release additional U to overlying waters similar to that observed over the Amazon River shelf.

Alternatively, the enhanced dissolved U concentrations in our study could be related to the El Niño Costero of 2017 (Echevin et al., 2018;Garreaud, 2018), which had developed rapidly and unexpectedly in January, and disappeared by May 2017 during cruise M136. The El Niño Costero had caused extreme impacts in Northern Peru with strong rainfall, severe flooding and landslides, which could deliver considerable amounts of dissolved and particulate U to our study area.

It is thus important to note that U concentrations in coastal systems are highly sensitive to weather conditions such as extreme rainfall and flooding, and bottom water oxygen concentrations, variability of which is expected to intensify with future climate change (Shepherd et al., 2017). Relatively minor variations in dissolved ^{238}U could account for substantial overestimation/underestimation of the depth-integrated ^{234}Th fluxes. We thus encourage future ^{234}Th flux studies in such environments to include seawater ^{238}U analysis.

3.2 Dynamic advective and diffusive ^{234}Th fluxes

The relative importance of ^{234}Th fluxes due to advection and diffusion were assessed here assuming steady state conditions, which assume negligible temporal ^{234}Th variability. But how valid is this assumption in the Peruvian upwelling zone? Repeat stations 495 and 516 show

https://doi.org/10.5194/bg-2020-57
Preprint. Discussion started: 9 March 2020

substantial temporal variations in ^{234}Th activities at each sampled depth in the top 200 m, while temperature and salinity profiles confirmed that similar water masses were sampled during both occupations (Figure 4). Particularly, the surface ^{234}Th deficit was more intense at St. 495 (^{234}Th/^{238}U = 0.44) compared to St. 516 (^{234}Th/^{238}U = 0.73). Correspondingly, ^{234}Th fluxes decreased substantially from St. 495 to St. 516. At 100 m, the difference in ^{234}Th fluxes between these two stations was ~ 30% (3200 ± 90 dpm m^{-2} d^{-1} at St. 495 and 2240 ± 110 dpm m^{-2} d^{-1} at St. 516). At 200 m where ^{234}Th resumed equilibrium with ^{238}U at both stations, ^{234}Th flux difference was ~ 25% (4510 ± 220 dpm m^{-2} d^{-1} at St. 495 and 3455 ± 200 dpm m^{-2} d^{-1} at St. 516). Taking the non-steady state term in Eq. (1) into consideration increased total ^{234}Th at St. 516 by 40% to 3110 ± 1870 dpm m^{-2} d^{-1} at 100 m (or 45% to 5040 ± 2290 dpm m^{-2} d^{-1} at 200 m), which is indistinguishable within error from fluxes at St. 495. However, the large errors associated with the non-steady state calculation prevent a meaningful application of this model in the current study (also see discussion in Resplandy et al, 2012). As estimation of the physical fluxes is independent of the models chosen between steady and non-steady states, the following discussion regarding physical effects on the ^{234}Th flux estimates is based on the steady state model only.

The significance of advection and diffusion in the total ^{234}Th flux budget highly depends on the upwelling rate, current velocity, vertical diffusivity, and ^{234}Th gradient on the horizontal and vertical directions. At nearshore stations, upwelling rates at the base of the mixed layer, derived from surface wind stress, ranged from a mere 1.3 × 10^{-7} m s^{-1} to 9.7 × 10^{-6} m s^{-1}, whereas upwelling rates at offshore stations were on the order of 10^{-10} m s^{-1} to 10^{-8} m s^{-1} and essentially negligible. As a result, upwelled ^{234}Th fluxes were only significant at stations closest to shore; these stations were 428, 883-12 and 904-16 whose upwelled ^{234}Th fluxes accounted for 10%,

https://doi.org/10.5194/bg-2020-57
Preprint. Discussion started: 9 March 2020

307 11% and 25% of the total ^{234}Th fluxes, respectively. Upwelled ^{234}Th fluxes were insignificant at
308 the rest of the stations.

309 Similarly, vertical diffusivities, shown as running mean over 20 m in Figure S1, were an
310 order of magnitude higher at shallow stations compared to those at deep stations. Within the 27 m
311 to 33 m layer at offshore stations, vertical diffusivities decrease exponentially by an order of
312 magnitude within a few meters; below this depth, vertical diffusivities remained relatively stable.
313 This is not surprising as wind-driven turbulent is most significant at the ocean surface
314 (Buckingham et al., 2019). In this study, the sampling depths immediately below the ML were
315 generally 30 m and 60 m. A few high vertical diffusivity values around 30 m at deep stations
316 were unlikely representative for the 30 m – 60 m water column layer. We thus opted to only
317 apply vertical diffusivities below 33 m at deep stations. Taken together, vertical diffusive ^{234}Th
318 fluxes at all deep stations appeared to be trivial in the total ^{234}Th flux budget (Figure 5). However,
319 at shallow stations 428, 458, and 883-12, vertical diffusive ^{234}Th fluxes made up 37%, 14%, and
320 21% of total ^{234}Th fluxes, respectively.

321 While calculation of the vertical ^{234}Th gradient is straightforward, the same is hardly true
322 for the determination of horizontal ^{234}Th gradient. Mean ^{234}Th in the top layer of the water
323 column is highly variable amongst stations (Table 3, Figure 6), and likely reflect variations
324 occurring at small temporal and spatial scales in the Peruvian OMZ. Quantification of the
325 horizontal ^{234}Th gradient between individual stations thus may not be adequate to evaluate large
326 scale advection and eddy diffusion across the study area. On a larger spatial scale, alongshore
327 ^{234}Th gradients at nearshore stations for M138 are fairly consistent, ranging from 1.5 x 10^{-6} dpm
328 L^{-1} m^{-1} to 1.7 x 10^{-6} dpm L^{-1} m^{-1}, with a slightly stronger gradient in the north compared to the
329 south. The net difference in alongshore ^{234}Th gradient is merely 2 x 10^{-7} dpm L^{-1} m^{-1}. A slightly

https://doi.org/10.5194/bg-2020-57
Preprint. Discussion started: 9 March 2020

smaller alongshore ^{234}Th gradient of 4.8 x 10^{-7} dpm L^{-1} m^{-1} was observed for M136. The magnitude of the net difference in alongshore ^{234}Th gradient during M136 cannot be adequately quantified, due to smaller spatial sampling coverage. Judging on the similarity in the spatial distributions of mean ^{234}Th between cruises M136 and M138, it is reasonable to assume that net difference in alongshore ^{234}Th gradient remained similar during both cruises. Correspondingly, average alongshore current velocities (Lüdke et al., in review 2019) for the surface layer varied from 0.06 m/s to 0.34 m/s. At the peripheral of a freshly-formed anticyclonic eddy (St. 915-1), alongshore current velocities could be as high as 0.53 m/s. Taking the mean alongshore velocity of 0.2 m/s, the resulting net horizontal advective ^{234}Th flux is ~ 50 dpm m^{-2} d^{-1}, a mere 3-9% of the total ^{234}Th fluxes and thus insignificant for the ^{234}Th flux budget.

Our findings are in reasonable agreement with those from the GEOTRACES GP16 eastern section along 12°S from Peru to Tahiti, in which Black et al. (2018) quantified both horizontal and vertical advective ^{234}Th fluxes. Horizontal advective fluxes for the upper 30 m water column estimated during GP16 were ~180 dpm m^{-2} d^{-1} for all nearshore and offshore stations, similar in magnitude to those estimated in our study. Upwelling fluxes along GP16 eastern section was suggested to account for 50% to 80% of total ^{234}Th fluxes at the base of the euphotic zone (at similar depths or slightly deeper than ML depths in the current study) (Black et al., 2018). Total ^{234}Th fluxes along the GP16 eastern section, ranging from 4000 to 5000 dpm m^{-2} d^{-1} at the base of the euphotic zone, were much higher than those in our study (560 to 1900 dpm m^{-2} d^{-1} at the base of the ML). This difference could be related to the period of sampling (austral autumn and winter 2017 in our study *vs.* austral summer 2013 for the GP16 section). We note that the estimated vertical mixing rates based on ^{7}Be isotope at the base of the euphotic zone along the GP16 section (Kadko, 2017) were at least an order of magnitude higher than the upwelling rates at the base of the ML at nearby stations in our study. This difference could stem from different

https://doi.org/10.5194/bg-2020-57
Preprint. Discussion started: 9 March 2020

methods used to estimate upwelling rates, and may also reflect the dynamic upwelling system off Peru in which upwelling rates vary greatly seasonally and interannually. During cruise M136 and M138, upwelling favorable easterly winds off Peru were weak, resulting in negligible coastal upwelling. Coastal upwelling in the same general area was also suggested to be negligible in austral summer 2013 during cruise M92 due to nominal surface wind stress (Thomsen et al., 2016). Results from studies conducted in the same year (October to December 2013, Kadko, 2017; December 2012, Steinfeldt et al., 2015) indicate that seasonal upwelling rates vary drastically in the Peruvian upwelling zone. The seasonal dynamics of coastal upwelling off Peru are similar to those seen in the Arabian Sea, where large upwelled ^{234}Th fluxes only occurred during mid-late southwest monsoon at stations close to shore (Buesseler et al., 1998). Our findings lend further support to earlier studies that advection and diffusion are seasonally important for ^{234}Th fluxes in regions with high upwelling velocities and diffusivities such as the equatorial Pacific (Bacon et al., 1996;Buesseler et al., 1995;Dunne and Murray, 1999) and coastal sites such as the Arabian Sea (Buesseler et al., 1998) and offshore Peru (Black et al., 2018; this study).

3.3 Residence time of ^{234}Th in the Peruvian OMZ

Residence time of total ^{234}Th represents a combination of the time required for the partition of dissolved ^{234}Th onto particulate matter and that for particle removal. In this study, residence time of total ^{234}Th in the surface layer (top 30 m during M136 and top 50 m during M138) varied from 20 days at shallow stations to 95 days at deep stations (mean $\tau = 51 \pm 23$ days, 1SD, n = 24; Table 3). These values were similar to those estimated within the California Current (Coale and Bruland, 1985) and the residence times of particulate organic carbon (POC)

https://doi.org/10.5194/bg-2020-57
Preprint. Discussion started: 9 March 2020

377 and nitrogen (PON) (Murray et al., 1989), but were much longer than predicted in nearshore shelf
378 waters where residence times of total ^{234}Th were on the order of a few days (Kaufman et al.,
379 1981;Kim et al., 1999; and references therein). The longer residence times estimated in our study
380 could reflect a combination of weak surface ^{234}Th deficits (^{234}Th = 0.63 to 1.82 dpm/L) (Figure 2)
381 and low export fluxes (800 to 2000 dpm m^{-2} d^{-1}, Figure 5). Nearshore seawater samples during
382 GP16 (Black et al., 2018) featured similar surface ^{234}Th deficits (^{234}Th = 0.63 to 1.33 dpm/L) but
383 much higher downward ^{234}Th fluxes (4000 to 5000 dpm m^{-2} d^{-1}) as a result of strong upwelling,
384 implying that residence times of total ^{234}Th in the Peruvian OMZ during GP16 occupation would
385 be 3 – 6 times shorter. Indeed, a quick re-assessment of the GP16 data predicted a shorter
386 residence time of total ^{234}Th of 5 – 23 days within the euphotic zone of the coastal Peruvian
387 OMZ.

388 These temporal variations on the residence times of total ^{234}Th have important
389 implications for the estimation of POC fluxes and quantification of carbon export efficiency.
390 Firstly, seasonal changes in Th residence times reflect variations in particle removal over
391 different integrated timescales. For example, POC produced in surface waters during GP16
392 (austral summer 2013) (Black et al., 2018) would have been exported out of the euphotic zone 3-
393 6 times faster than it did during austral autumn 2017 (this study). Secondly, to properly evaluate
394 carbon export efficiency, surface net primary production (NPP) should be averaged over a similar
395 timescale as the residence time of total ^{234}Th during station occupation. Applying a 16-day
396 averaged NPP for export efficiency estimate (Black et al., 2018;Henson et al., 2011) would likely
397 not be appropriate in the current study in which total ^{234}Th fluxes integrated timescales of several
398 weeks. ^{234}Th residence times should thus be properly quantified in coastal studies before deriving
399 export efficiencies over varying NPP integration timescales.

https://doi.org/10.5194/bg-2020-57
Preprint. Discussion started: 9 March 2020

400

401 **4. Conclusions and implications for coastal ^{234}Th flux studies**

402 Advection and diffusion are important in coastal and upwelling regions with respect to
403 ^{234}Th export fluxes (Bacon et al., 1996;Buesseler et al., 1995;Dunne and Murray, 1999;Buesseler
404 et al., 1998). Our findings show that their significance is subject to the seasonal variability of the
405 current and upwelling velocities, diffusivities and ^{234}Th gradients, and should be evaluated on a
406 case-to-case basis. Advective fluxes are perhaps the most straightforward to estimate as current
407 velocities can be obtained routinely from shipboard ADCP measurements and upwelling rates
408 calculated from satellite wind stress (Steinfeldt et al., 2015;Bacon et al., 1996). Horizontal and
409 vertical velocities derived from general ocean circulation models also provide a good first order
410 estimate for advective ^{234}Th fluxes; this approach has been successfully demonstrated in a few
411 studies (Buesseler et al., 1995;Buesseler et al., 1998). In addition, the anthropogenic SF_6 tracer
412 and radium isotopes, widely used to quantify nutrient and Fe fluxes (Charette et al., 2007;Law et
413 al., 2001), could be used independently to constrain horizontal and vertical exchange rates of
414 ^{234}Th (Morris et al., 2007;Charette et al., 2007;Buesseler et al., 2005). When *in situ*
415 microstructure measurements are available (this study), vertical diffusivity can be directly
416 calculated to estimate the vertical diffusive ^{234}Th fluxes. Yet, microstructure analysis is not a
417 routine measurement on oceanographic cruises. Earlier studies in the equatorial Pacific and the
418 Gulf of Maine have shown that general ocean circulation models and a simple assumption on
419 dissipation coefficients could provide a robust estimate on vertical and horizontal diffusivities
420 (Benitez-Nelson et al., 2000;Gustafsson et al., 1998;Charette et al., 2001). Therefore, the
421 calculation of physical fluxes is possible, though challenging, and ^{234}Th fluxes due to physical

https://doi.org/10.5194/bg-2020-57
Preprint. Discussion started: 9 March 2020

422 processes should be carefully considered when conducting research in a coastal and upwelling
423 systems.

424 A striking finding in this study is that the assumption of a linear ^{238}U-S correlation could
425 lead to one of the largest errors in ^{234}Th flux estimates. In our study, using the S-based ^{238}U
426 activities resulted in significant underestimation of total ^{234}Th fluxes by as much as 40%. Because
427 the translation of ^{238}U activities to ^{234}Th fluxes is not linear, larger differences between measured
428 and S-based ^{238}U do not necessarily contribute to greater overestimation or underestimation of
429 ^{234}Th fluxes. For example, moderate difference of 3-6% in ^{238}U throughout the upper 100 m at
430 station 898 lead to 40% difference in final ^{234}Th flux, while a 5-9% difference in ^{238}U at station
431 906 only resulted in 16% ^{234}Th flux difference (Table 2, S2). We would thus stress the
432 importance of ^{238}U measurements in future ^{234}Th flux studies particularly in coastal and shelf
433 regions.

434 Finally, our study showed that the residence times of total ^{234}Th in the Peruvian nearshore
435 waters varied seasonally. Tropical OMZs are important hotpots for carbon sequestration from the
436 atmosphere and enhanced sedimentary carbon preservation (Arthur et al., 1998;Suess et al.,
437 1987). These OMZs are projected to intensify as a result of future climate change (Keeling and
438 Garcia, 2002;Schmidtko et al., 2017;Stramma et al., 2008). Future studies should take into
439 consideration the large temporal variations of the residence times of total ^{234}Th in order to
440 properly evaluates how carbon biogeochemical cycles and carbon export efficiency in these
441 OMZs will respond to continuing ocean deoxygenation,

442

443 **Data availability**

https://doi.org/10.5194/bg-2020-57
Preprint. Discussion started: 9 March 2020

Data are available in supplementary tables and will be archived in Pangea upon publication of the article.

Author contribution

RCX, FACLM and EAP designed the study. RCX carried out sampling, on-board beta counting of ^{234}Th, and drafted the manuscript. IR conducted ^{234}Th and ^{238}U analyses at home laboratory. JL computed current velocities and vertical diffusivities respectively from VmADCP and microstructure profiler data. All co-authors had a chance to review the manuscript and contributed to discussion and interpretation of the data presented.

Competing interests

The authors declare that they have no conflict of interest.

Acknowledgements

We thank the crew and science party on board M136 and M138 for their help in sample collection and instrument operation. Thank you to SiaoJean Ko, Dominik Jasinski, André Mutzberg and Mario Esposito for their laboratory assistance. The project, cruises, IR, JL and RCX were funded by the German SFB 754 program (‘Climate-Biogeochemistry Interactions in the Tropical Ocean’), and FACLM by a DFG Fellowship of the Excellence Cluster “The Future Ocean” (CP1403). This manuscript benefited from stimulating discussions at the BIARRITZ (‘bridging

https://doi.org/10.5194/bg-2020-57
Preprint. Discussion started: 9 March 2020

464 international activity and related research into the twilight zone') workshop held in Southampton,

465 UK in 2019.

https://doi.org/10.5194/bg-2020-57
Preprint. Discussion started: 9 March 2020

References

Abernathey, R. P., and Marshall, J.: Global surface eddy diffusivities derived from satellite altimetry, Journal of Geophysical Research: Oceans, 118, 901-916, https://doi.org/10.1002/jgrc.20066, 2013.

Anderson, R. F., Fleisher, M. Q., and LeHuray, A. P.: Concentration, oxidation state, and particulate flux of uranium in the Black Sea, Geochimica et Cosmochimica Acta, 53, 2215-2224, https://doi.org/10.1016/0016-7037(89)90345-1, 1989.

Arthur, M. A., Dean, W. E., and Laarkamp, K.: Organic carbon accumulation and preservation in surface sediments on the Peru margin, Chemical Geology, 152, 273-286, https://doi.org/10.1016/S0009-2541(98)00120-X, 1998.

Bacon, M., Cochran, J., Hirschberg, D., Hammar, T., and Fleer, A.: Export flux of carbon at the equator during the EqPac time-series cruises estimated from 234Th measurements, Deep Sea Research Part II: Topical Studies in Oceanography, 43, 1133-1153, https://doi.org/10.1016/0967-0645(96)00016-1, 1996.

Barnes, C. E., and Cochran, J. K.: Uranium geochemistry in estuarine sediments: Controls on removal and release processes, Geochimica et Cosmochimica Acta, 57, 555-569, https://doi.org/10.1016/0016-7037(93)90367-6, 1993.

Benitez-Nelson, C. R., Buesseler, K. O., and Crossin, G.: Upper ocean carbon export, horizontal transport, and vertical eddy diffusivity in the southwestern Gulf of Maine, Continental Shelf Research, 20, 707-736, https://doi.org/10.1016/S0278-4343(99)00093-X, 2000.

Bentamy, A., and Croize-Fillon: Gridded surface wind fields from Metop/ASCAT measurements, International Journal of Remote Sensing, doi:10.1080/01431161.2011.600348, 2010.

Bhat, S., Krishnaswamy, S., Lal, D., and Moore, W.: 234Th/238U ratios in the ocean, Earth and Planetary Science Letters, 5, 483-491, 1968.

https://doi.org/10.5194/bg-2020-57
Preprint. Discussion started: 9 March 2020

491 Black, E. E., Buesseler, K. O., Pike, S. M., and Lam, P. J.: 234Th as a tracer of particulate export
492 and remineralization in the southeastern tropical Pacific, Marine Chemistry, 201, 35-50,
493 https://doi.org/10.1016/j.marchem.2017.06.009, 2018.
494 Black, E. E., Lam, P. J., Lee, J. M., and Buesseler, K. O.: Insights From the 238U - 234Th
495 Method Into the Coupling of Biological Export and the Cycling of Cadmium, Cobalt, and
496 Manganese in the Southeast Pacific Ocean, Global Biogeochemical Cycles, 33, 15-36,
497 https://doi.org/10.1029/2018GB005985, 2019.
498 Buckingham, C. E., Lucas, N. S., Belcher, S. E., Rippeth, T. P., Grant, A. L. M., Le Sommer, J.,
499 Ajayi, A. O., and Naveira Garabato, A. C.: The Contribution of Surface and Submesoscale
500 Processes to Turbulence in the Open Ocean Surface Boundary Layer, Journal of Advances in
501 Modeling Earth Systems, 11, 4066-4094, https://doi.org/10.1029/2019MS001801, 2019.
502 Buesseler, K., Ball, L., Andrews, J., Benitez-Nelson, C., Belastock, R., Chai, F., and Chao, Y.:
503 Upper ocean export of particulate organic carbon in the Arabian Sea derived from thorium-234,
504 Deep Sea Research Part II: Topical Studies in Oceanography, 45, 2461-2487,
505 https://doi.org/10.1016/S0967-0645(98)80022-2, 1998.
506 Buesseler, K. O., Bacon, M. P., Cochran, J. K., and Livingston, H. D.: Carbon and nitrogen
507 export during the JGOFS North Atlantic Bloom Experiment estimated from 234Th: 238U
508 disequilibria, Deep Sea Research Part A. Oceanographic Research Papers, 39, 1115-1137,
509 https://doi.org/10.1016/0198-0149(92)90060-7, 1992.
510 Buesseler, K. O., Andrews, J. A., Hartman, M. C., Belastock, R., and Chai, F.: Regional estimates
511 of the export flux of particulate organic carbon derived from thorium-234 during the JGOFS
512 EqPac program, Deep Sea Research Part II: Topical Studies in Oceanography, 42, 777-804,
513 https://doi.org/10.1016/0967-0645(95)00043-P, 1995.

https://doi.org/10.5194/bg-2020-57
Preprint. Discussion started: 9 March 2020

514 Buesseler, K. O., Andrews, J., Pike, S. M., Charette, M. A., Goldson, L. E., Brzezinski, M. A.,
515 and Lance, V.: Particle export during the southern ocean iron experiment (SOFeX), Limnology
516 and Oceanography, 50, 311-327, https://doi.org/10.4319/lo.2005.50.1.0311, 2005.
517 Buesseler, K. O., Benitez-Nelson, C. R., Moran, S., Burd, A., Charette, M., Cochran, J. K.,
518 Coppola, L., Fisher, N., Fowler, S., and Gardner, W.: An assessment of particulate organic carbon
519 to thorium-234 ratios in the ocean and their impact on the application of 234Th as a POC flux
520 proxy, Marine Chemistry, 100, 213-233, https://doi.org/10.1016/j.marchem.2005.10.013, 2006.
521 Buesseler, K. O., and Boyd, P. W.: Shedding light on processes that control particle export and
522 flux attenuation in the twilight zone of the open ocean, Limnology and Oceanography, 54, 1210-
523 1232, https://doi.org/10.4319/lo.2009.54.4.1210, 2009.
524 Cai, P., Chen, W., Dai, M., Wan, Z., Wang, D., Li, Q., Tang, T., and Lv, D.: A high‐resolution
525 study of particle export in the southern South China Sea based on 234Th: 238U disequilibrium,
526 Journal of Geophysical Research: Oceans, 113, 2008.
527 Charette, M. A., Moran, S. B., Pike, S. M., and Smith, J. N.: Investigating the carbon cycle in the
528 Gulf of Maine using the natural tracer thorium 234, Journal of Geophysical Research: Oceans,
529 106, 11553-11579, https://doi.org/10.1029/1999JC000277, 2001.
530 Charette, M. A., Gonneea, M. E., Morris, P. J., Statham, P., Fones, G., Planquette, H., Salter, I.,
531 and Garabato, A. N.: Radium isotopes as tracers of iron sources fueling a Southern Ocean
532 phytoplankton bloom, Deep Sea Research Part II: Topical Studies in Oceanography, 54, 1989-
533 1998, https://doi.org/10.1016/j.dsr2.2007.06.003, 2007.
534 Chen, J., Edwards, R. L., and Wasserburg, G. J.: 238U, 234U and232Th in seawater, Earth and
535 Planetary Science Letters, 80, 241-251, https://doi.org/10.1016/0012-821X(86)90108-1, 1986.
536 Coale, K. H., and Bruland, K. W.: 234Th: 238U disequilibria within the California Current 1,
537 Limnology and Oceanography, 30, 22-33, https://doi.org/10.4319/lo.1985.30.1.0022, 1985.

538 Coale, K. H., and Bruland, K. W.: Oceanic stratified euphotic zone as elucidated by 234Th: 238U
539 disequilibria 1, Limnology and Oceanography, 32, 189-200,
540 https://doi.org/10.4319/lo.1987.32.1.0189, 1987.
541 Cochran, J.: The oceanic chemistry of the uranium-and thorium-series nuclides, in: Uranium-
542 series disequilibrium: applications to earth, marine, and environmental sciences. 2. ed, 1992.
543 Cochran, J., and Masqué, P.: Short-lived U/Th series radionuclides in the ocean: tracers for
544 scavenging rates, export fluxes and particle dynamics, Reviews in Mineralogy and geochemistry,
545 52, 461-492, https://doi.org/10.2113/0520461, 2003.
546 Dunne, J. P., and Murray, J. W.: Sensitivity of 234Th export to physical processes in the central
547 equatorial Pacific, Deep Sea Research Part I: Oceanographic Research Papers, 46, 831-854,
548 https://doi.org/10.1016/S0967-0637(98)00098-3, 1999.
549 Echevin, V. M., Colas, F., Espinoza-Morriberon, D., Anculle, T., Vasquez, L., and Gutierrez, D.:
550 Forcings and evolution of the 2017 coastal El Niño off Northern Peru and Ecuador, Frontiers in
551 Marine Science, 5, 367, https://doi.org/10.3389/fmars.2018.00367, 2018.
552 Fischer, T., Banyte, D., Brandt, P., Dengler, M., Krahmann, G., Tanhua, T., and Visbeck, M.:
553 Diapycnal oxygen supply to the tropical North Atlantic oxygen minimum zone, Biogeosciences,
554 10, 5079-5093, https://doi.org/10.5194/bg-10-5079-2013, 2013.
555 Garreaud, R. D.: A plausible atmospheric trigger for the 2017 coastal El Niño, International
556 Journal of Climatology, 38, e1296-e1302, https://doi.org/10.1002/joc.5426, 2018.
557 Gustafsson, Ö., Buesseler, K. O., Rockwell Geyer, W., Bradley Moran, S., and Gschwend, P. M.:
558 An assessment of the relative importance of horizontal and vertical transport of particle-reactive
559 chemicals in the coastal ocean, Continental Shelf Research, 18, 805-829,
560 https://doi.org/10.1016/S0278-4343(98)00015-6, 1998.

https://doi.org/10.5194/bg-2020-57
Preprint. Discussion started: 9 March 2020

561 Hahn, J., Brandt, P., Greatbatch, R. J., Krahmann, G., and Körtzinger, A.: Oxygen variance and
562 meridional oxygen supply in the Tropical North East Atlantic oxygen minimum zone, Climate
563 dynamics, 43, 2999-3024, https://doi.org/10.1007/s00382-014-2065-0, 2014.
564 Henson, S. A., Sanders, R., Madsen, E., Morris, P. J., Le Moigne, F., and Quartly, G. D.: A
565 reduced estimate of the strength of the ocean's biological carbon pump, Geophysical Research
566 Letters, 38, 10.1029/2011gl046735, 2011.
567 Kadko, D.: Upwelling and primary production during the US GEOTRACES East Pacific Zonal
568 Transect, Global Biogeochemical Cycles, 31, 218-232, https://doi.org/10.1002/2016GB005554,
569 2017.
570 Kaufman, A., Li, Y.-H., and Turekian, K. K.: The removal rates of234Th and228Th from waters
571 of the New York Bight, Earth and Planetary Science Letters, 54, 385-392,
572 https://doi.org/10.1016/0012-821X(81)90054-6, 1981.
573 Keeling, R. F., and Garcia, H. E.: The change in oceanic O2 inventory associated with recent
574 global warming, Proceedings of the National Academy of Sciences, 99, 7848-7853,
575 10.1073/pnas.122154899, 2002.
576 Kim, G., Hussain, N., and Church, T. M.: How accurate are the 234Th based particulate residence
577 times in the ocean?, Geophysical research letters, 26, 619-622,
578 https://doi.org/10.1029/1999GL900037, 1999.
579 Ku, T.-L., Knauss, K. G., and Mathieu, G. G.: Uranium in open ocean: concentration and isotopic
580 composition, Deep Sea Research, 24, 1005-1017, https://doi.org/10.1016/0146-6291(77)90571-9,
581 1977.
582 Law, C., Martin, A., Liddicoat, M., Watson, A., Richards, K., and Woodward, E.: A Lagrangian
583 SF6 tracer study of an anticyclonic eddy in the North Atlantic: Patch evolution, vertical mixing

584 and nutrient supply to the mixed layer, Deep Sea Research Part II: Topical Studies in
585 Oceanography, 48, 705-724, https://doi.org/10.1016/S0967-0645(00)00112-0, 2001.
586 Le Moigne, F. A. C., Henson, S. A., Sanders, R. J., and Madsen, E.: Global database of surface
587 ocean particulate organic carbon export fluxes diagnosed from the </sup>234</sup>Th
588 technique, Earth Syst. Sci. Data, 5, 295-304, https://doi.org/10.5194/essd-5-295-2013, 2013.
589 Lee, C., Murray, D., Barber, R., Buesseler, K., Dymond, J., Hedges, J., Honjo, S., Manganini, S.,
590 Marra, J., and Moser, C.: Particulate organic carbon fluxes: compilation of results from the 1995
591 US JGOFS Arabian Sea process study: By the Arabian Sea carbon flux group, Deep Sea
592 Research Part II: Topical Studies in Oceanography, 45, 2489-2501,
593 https://doi.org/10.1016/S0967-0645(98)00079-4, 1998.
594 Lüdke, J., Dengler, M., Sommer, S., Clemens, D., Thomsen, S., Krahmann, G., Dale, A. W.,
595 Achterberg, E. P., and Visbeck, M.: Influence of intraseasonal eastern boundary circulation
596 variability on hydrography and biogeochemistry off Peru, Ocean Sci. Discuss., 2019, 1-31,
597 https://doi.org/10.5194/os-2019-93, in review 2019.
598 McKee, B. A., DeMaster, D. J., and Nittrouer, C. A.: Uranium geochemistry on the Amazon
599 shelf: evidence for uranium release from bottom sediments, Geochimica et Cosmochimica Acta,
600 51, 2779-2786, https://doi.org/10.1016/0016-7037(87)90157-8, 1987.
601 Moore, W.: Radionuclides of the uranium and thorium decay series in the estuarine environment,
602 in: Uranium-series disequilibrium: applications to earth, marine, and environmental sciences. 2.
603 ed, 1992.
604 Morris, P. J., Sanders, R., Turnewitsch, R., and Thomalla, S.: 234Th-derived particulate organic
605 carbon export from an island-induced phytoplankton bloom in the Southern Ocean, Deep Sea
606 Research Part II: Topical Studies in Oceanography, 54, 2208-2232,
607 https://doi.org/10.1016/j.dsr2.2007.06.002, 2007.

608 Murray, J. W., Downs, J. N., Strom, S., Wei, C.-L., and Jannasch, H. W.: Nutrient assimilation,
609 export production and 234Th scavenging in the eastern equatorial Pacific, Deep Sea Research
610 Part A. Oceanographic Research Papers, 36, 1471-1489, https://doi.org/10.1016/0198-
611 0149(89)90052-6, 1989.
612 Noffke, A., Hensen, C., Sommer, S., Scholz, F., Bohlen, L., Mosch, T., Graco, M., and
613 Wallmann, K.: Benthic iron and phosphorus fluxes across the Peruvian oxygen minimum zone,
614 Limnology and Oceanography, 57, 851-867, https://doi.org/10.4319/lo.2012.57.3.0851, 2012.
615 Owens, S., Buesseler, K., and Sims, K.: Re-evaluating the 238U-salinity relationship in seawater:
616 Implications for the 238U–234Th disequilibrium method, Marine Chemistry, 127, 31-39,
617 https://doi.org/10.1016/j.marchem.2011.07.005, 2011.
618 Owens, S. A., Pike, S., and Buesseler, K. O.: Thorium-234 as a tracer of particle dynamics and
619 upper ocean export in the Atlantic Ocean, Deep Sea Research Part II: Topical Studies in
620 Oceanography, 116, 42-59, http://dx.doi.org/10.1016/j.dsr2.2014.11.010, 2015.
621 Pike, S., Buesseler, K., Andrews, J., and Savoye, N.: Quantification of 234 Th recovery in small
622 volume sea water samples by inductively coupled plasma-mass spectrometry, Journal of
623 Radioanalytical and Nuclear Chemistry, 263, 355-360, https://doi.org/10.1007/s10967-005-0594-
624 z, 2005.
625 Rengarajan, R., Sarin, M., and Krishnaswami, S.: Uranium in the Arabian Sea: role of
626 denitrification in controlling its distribution, Oceanologica acta, 26, 687-693,
627 https://doi.org/10.1016/j.oceact.2003.05.001, 2003.
628 Rosengard, S. Z., Lam, P. J., Balch, W. M., Auro, M. E., Pike, S., Drapeau, D., and Bowler, B.:
629 Carbon export and transfer to depth across the Southern Ocean Great Calcite Belt,
630 doi:10.5194/bg-12-3953-2015, 2015.

https://doi.org/10.5194/bg-2020-57
Preprint. Discussion started: 9 March 2020

631 Savoye, N., Benitez-Nelson, C., Burd, A. B., Cochran, J. K., Charette, M., Buesseler, K. O.,
632 Jackson, G. A., Roy-Barman, M., Schmidt, S., and Elskens, M.: 234Th sorption and export
633 models in the water column: a review, Marine Chemistry, 100, 234-249,
634 https://doi.org/10.1016/j.marchem.2005.10.014, 2006.
635 Schmidt, S., and Reyss, J.: Uranium concentrations of Mediterranean seawater with high
636 salinities, Comptes Rendus de l'Academie des Sciences. Serie 2, 312, 479-484, 1991.
637 Schmidtko, S., Stramma, L., and Visbeck, M.: Decline in global oceanic oxygen content during
638 the past five decades, Nature, 542, 335, 10.1038/nature21399, 2017.
639 Scholz, F., McManus, J., Mix, A. C., Hensen, C., and Schneider, R. R.: The impact of ocean
640 deoxygenation on iron release from continental margin sediments, Nature Geosci, 7, 433-437,
641 https://doi.org/10.1038/ngeo2162, 2014.
642 Steinfeldt, R., Sültenfuß, J., Dengler, M., Fischer, T., and Rhein, M.: Coastal upwelling off Peru
643 and Mauritania inferred from helium isotope disequilibrium, Biogeosciences, 12, 7519-7533,
644 https://doi.org/10.5194/bg-12-7519-2015, 2015.
645 Stramma, L., Johnson, G. C., Sprintall, J., and Mohrholz, V.: Expanding oxygen-minimum zones
646 in the tropical oceans, science, 320, 655-658, 2008.
647 Suess, E., Kulm, L., and Killingley, J.: Coastal upwelling and a history of organic-rich mudstone
648 deposition off Peru, Geological Society, London, Special Publications, 26, 181-197, 1987.
649 Swarzenski, P., Campbell, P., Porcelli, D., and McKee, B.: The estuarine chemistry and isotope
650 systematics of 234,238 U in the Amazon and Fly Rivers, Continental Shelf Research, 24, 2357-
651 2372, https://doi.org/10.1016/j.csr.2004.07.025, 2004.
652 Swarzenski, P. W., Porcelli, D., Andersson, P. S., and Smoak, J. M.: The behavior of U-and Th-
653 series nuclides in the estuarine environment, Reviews in Mineralogy and Geochemistry, 52, 577-
654 606, https://doi.org/10.2113/0520577, 2003.

https://doi.org/10.5194/bg-2020-57
Preprint. Discussion started: 9 March 2020

655 Thomsen, S., Kanzow, T., Krahmann, G., Greatbatch, R. J., Dengler, M., and Lavik, G.: The
656 formation of a subsurface anticyclonic eddy in the Peru‐Chile Undercurrent and its impact on
657 the near‐coastal salinity, oxygen, and nutrient distributions, Journal of Geophysical Research:
658 Oceans, 121, 476-501, https://doi.org/10.1002/2015JC010878, 2016.
659 Van Der Loeff, M. R., Sarin, M. M., Baskaran, M., Benitez-Nelson, C., Buesseler, K. O.,
660 Charette, M., Dai, M., Gustafsson, Ö., Masque, P., and Morris, P. J.: A review of present
661 techniques and methodological advances in analyzing 234Th in aquatic systems, Marine
662 Chemistry, 100, 190-212, https://doi.org/10.1016/j.marchem.2005.10.012, 2006.
663 Waples, J. T., Benitez-Nelson, C., Savoye, N., van der Loeff, M. R., Baskaran, M., and
664 Gustafsson, Ö.: An introduction to the application and future use of 234Th in aquatic systems,
665 Marine Chemistry, 100, 166-189, https://doi.org/10.1016/j.marchem.2005.10.011, 2006.
666 Weinstein, S. E., and Moran, S. B.: Vertical flux of particulate Al, Fe, Pb, and Ba from the upper
667 ocean estimated from 234Th/238U disequilibria, Deep Sea Research Part I: Oceanographic
668 Research Papers, 52, 1477-1488, https://doi.org/10.1016/j.dsr.2005.03.008, 2005.
669 Zhurbas, V., and Oh, I. S.: Drifter‐derived maps of lateral diffusivity in the Pacific and Atlantic
670 oceans in relation to surface circulation patterns, Journal of Geophysical Research: Oceans, 109,
671 https://doi.org/10.1029/2003JC002241, 2004.

672

673

https://doi.org/10.5194/bg-2020-57
Preprint. Discussion started: 9 March 2020

674 Figure captions

675 Figure 1. Map showing locations of each station from M136 (white squares) and M138 (grey
676 circles). Color boxes schematically divide the four shore-normal transects. This map was created
677 with Ocean Data View (Schlitzer, 2014).

678

679 Figure 2. Profiles of ^{238}U (black) and ^{234}Th (orange squares – M136; orange circles –M138) along
680 with concentrations of oxygen (grey) and fluorescence (green). Profiles are organized by cruises,
681 transects, and distance to shore from left to right and top to bottom.

682

683 Figure 3. Cross plots of measured ^{238}U activities vs. salinity for M136 (a) and M138 (b), showing
684 poor linear relationship between ^{238}U and salinity. (c) shows a direct comparison between
685 measured and salinity-based ^{238}U to further highlight the large difference between the two. The
686 solid blue line indicates the 1:1 ratio between measured and projected ^{238}U. Blue dashed lines
687 indicate the ± errors reported in Owens et al. (2011).

688

689 Figure 4. Profiles of repeated stations for (a) temperature (solid lines) and salinity (dashed lines)
690 for St. 495 (blue) and St. 516 (orange); (b) and (c) profiles of ^{238}U (black), ^{234}Th (color squares),
691 and concentrations of oxygen (grey) and fluorescence (green).

692

693 Figure 5. Bar charts of ^{234}Th fluxes due to production and decay (blue), upwelling (orange), and
694 vertical diffusion (grey) for the base of the ML (top) and 100 m (bottom). Color boxes

https://doi.org/10.5194/bg-2020-57
Preprint. Discussion started: 9 March 2020

695 corresponds to individual transects in Figure 1. Within each transect stations from west (offshore)
696 to east (nearshore) are listed from left to right. Error bars (1SE) were indicated.

697

698 Figure 6. Distributions of averaged ^{234}Th activities during M136 (a, top 30 m) and M138 (b, top
699 50 m).

https://doi.org/10.5194/bg-2020-57
Preprint. Discussion started: 9 March 2020

Table 1. ^{234}Th fluxes due to production and decay, upwelling and vertical diffusion below the mixed layer and at 100 m. Horizontal advective fluxes were not quantified at 100 m. Refer to text for details.

							^{234}Th flux at the base of the ML					^{234}Th flux at 100 m				
Cruise	Station	Cast	Mixed layer depth	Upper oxycline depth	Maximum fluorescence	Equilibrium depth	Depth	Production and decay	Upwelling	Diffusion	Final flux	1 SD	Production and decay	Upwelling	Diffusion	Final flux	1 SD
			m	m	µg L^{-1}	m	m	dpm m^{-2} d^{-1}	dpm m^{-2} d^{-1}	dpm m^{-2} d^{-1}	dpm m^{-2} d^{-1}	dpm m^{-2} d^{-1}	dpm m^{-2} d^{-1}	dpm m^{-2} d^{-1}	dpm m^{-2} d^{-1}	dpm m^{-2} d^{-1}	dpm m^{-2} d^{-1}
M136	353	1	25	102	1.20	100	30	907	52	-36	923	69	1422	-14	2	1410	189
M136	380	1	26	129	0.87	80	30	1145	0	-41	1105	54	1637	0	-1	1637	132
M136	402	1	24	129	7.51	100	30	808	0	-75	732	64	1234	0	2	1236	111
M136	428	1	10	76	4.11	30	30	983	-128	493	1348	129	1772	33	-390	1415	256
M136	445	1	17	64	2.07	100	30	820	-10	16	826	66	1621	53	6	1681	165
M136	458	1	5	55	1.61	100	30	1012	-18	161	1155	117	2101	-11	145	2235	238
M136	472	1	11	29	7.41	200	40	1887	15	-29	1872	77	3315	-12	63	3366	233
M136	495	1	18	50	1.13	200	30	1149	1	-19	1130	50	3195	2	-5	3192	89
M136	516	1	16	45	3.77	200	30	614	0	1	615	49	2229	2	-4	2227	109
M136	547	1	22	48	1.28	150	30	791	0	85	877	61	2510	0	-15	2495	118
M136	559	1	20	79	1.70	85	50	623	3	-67	559	117	854	-4	2	852	120
M136	567	1	21	50	2.40	150	30	1593	0	-23	1570	52	3011	0	-11	3000	86
M138	879	3	43	93	2.24	200	60	1249	0	-16	1266	91	1702	0	-5	1697	111
M138	882	10	39	211	2.68	150	50	1321	-7	16	1331	63	2264	19	-12	2272	82
M138	883	12	10	220	1.31	250	30	683	-84	-159	758	108	1782	31	-121	1692	179
M138	888	7	41	127	1.59	150	50	1364	0	-120	1244	62	1813	0	-4	1809	86
M138	892	14	47	128	1.05	100	60	1395	33	-118	1309	72	1743	-3	1	1741	99
M138	898	1	38	101	1.42	60	50	1099	0	-19	1080	104	1091	0	0	1091	125
M138	904	16	12	72	3.63	150	20	812	275	0	1087	76	2643	0	-9	2634	79
M138	906	18	32	81	1.73	200	40	1796	0	4	1799	41	3100	0	-1	3100	77
M138	907	11	31	100	1.29	60	60	1594	-88	13	1518	147	1787	67	-2	1853	140
M138	912	3	37	70	2.75	>600	50	1960	0	-79	1881	43	2975	0	-3	2972	78
M138	915	1	26	99	3.51	200	40	1628	0	22	1650	38	2752	0	0	2752	93
M138	919	1	19	79	4.46	150	30	1316	0	49	1365	32	3249	0	-8	3241	85

https://doi.org/10.5194/bg-2020-57
Preprint. Discussion started: 9 March 2020

Table 2. Comparison of ^{234}Th fluxes at 100 m calculated with measured ^{238}U activities and those with salinity-based ^{238}U.

Cruise	Station	Cast	^{234}Th fluxes at 100 m* measured dpm m^{-2} d^{-1}	predicted dpm m^{-2} d^{-1}	Difference %
M136	353	1	1422	1320	8
M136	380	1	1637	1304	26
M136	402	1	1234	865	43
M136	428	1	1772	1443	23
M136	445	1	1621	1365	19
M136	458	1	2101	1859	13
M136	472	1	3315	3073	8
M136	495	1	3195	3058	4
M136	516	1	2229	2140	4
M136	547	1	2510	2313	9
M136	559	1	854	751	14
M136	567	1	3011	2879	5
M138	879	3	1702	1515	12
M138	882	10	2264	1875	21
M138	883	12	1782	1352	32
M138	888	7	1813	1441	26
M138	892	14	1743	1257	39
M138	898	1	1091	770	42
M138	904	16	2643	2280	16
M138	906	18	3100	2673	16
M138	907	11	1787	1308	37
M138	912	3	2975	2572	16
M138	915	1	2752	2380	16
M138	919	1	3249	2862	14

* For comparison purposes, we only report here ^{234}Th fluxes due to radioactive production and decay.

https://doi.org/10.5194/bg-2020-57
Preprint. Discussion started: 9 March 2020

Table 3. Residence time of total ^{234}Th in the surface layers of Peruvian OMZ.

Cruise	Station	Cast	Average ^{234}Th in the surface layer* dpm L^{-1}	Residence time days
M136	353	1	1.48	46
M136	380	1	1.35	35
M136	402	1	1.64	61
M136	428	1	1.57	35
M136	445	1	1.64	61
M136	458	1	1.45	38
M136	472	1	0.93	20
M136	495	1	1.20	31
M136	516	1	1.74	85
M136	547	1	1.67	63
M136	559	1	1.75	94
M136	567	1	1.41	45
M138	879	3	1.59	75
M138	882	10	1.81	69
M138	883	12	1.87	74
M138	888	7	1.68	67
M138	892	14	1.69	65
M138	898	1	1.66	92
M138	904	16	1.32	24
M138	906	18	1.15	25
M138	907	11	1.04	41
M138	912	3	1.25	33
M138	915	1	1.16	28
M138	919	1	1.17	26

* Here 'surface layer' refers to the top 30 m during M136 and top 50 m during M138.

https://doi.org/10.5194/bg-2020-57
Preprint. Discussion started: 9 March 2020

Biogeosciences
Discussions
Open Access
EGU

Figure 1

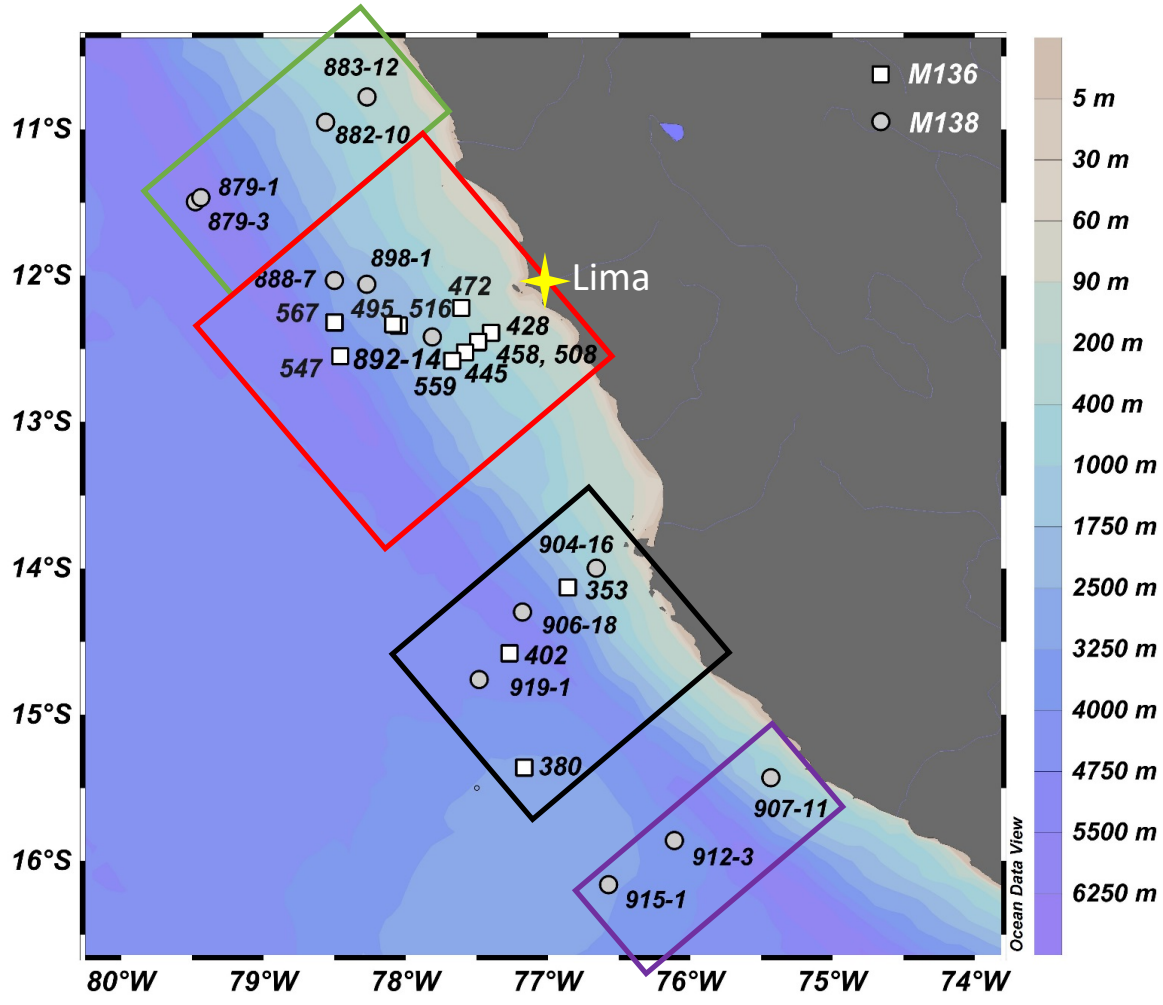

https://doi.org/10.5194/bg-2020-57
Preprint. Discussion started: 9 March 2020

Biogeosciences
Discussions
Open Access
EGU

Figure 2

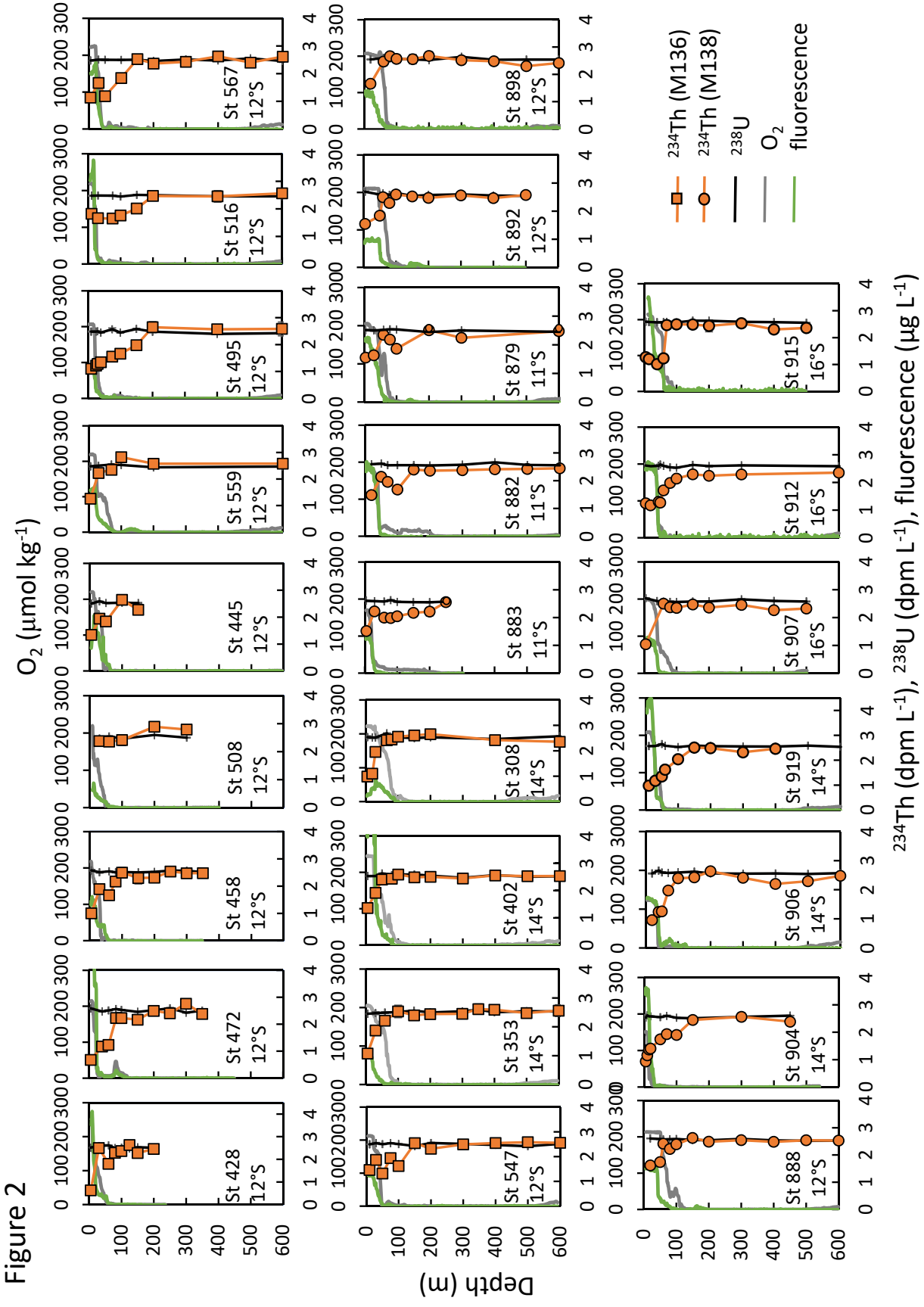

https://doi.org/10.5194/bg-2020-57
Preprint. Discussion started: 9 March 2020

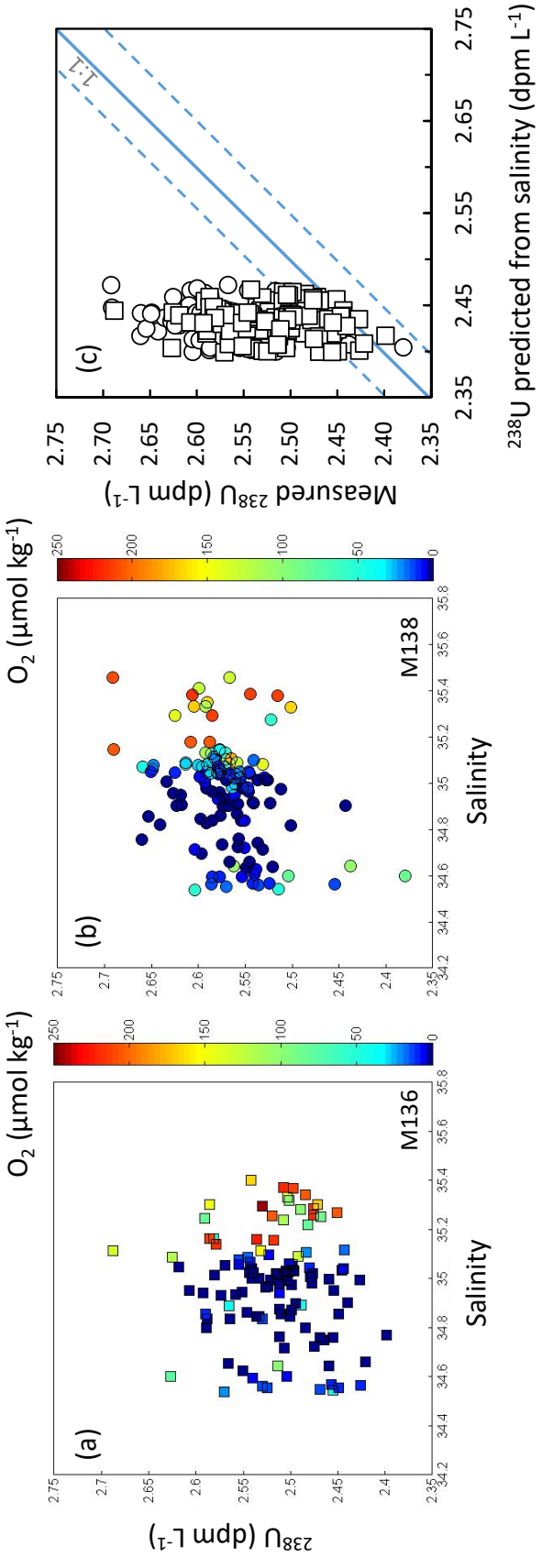

Figure 3

https://doi.org/10.5194/bg-2020-57
Preprint. Discussion started: 9 March 2020

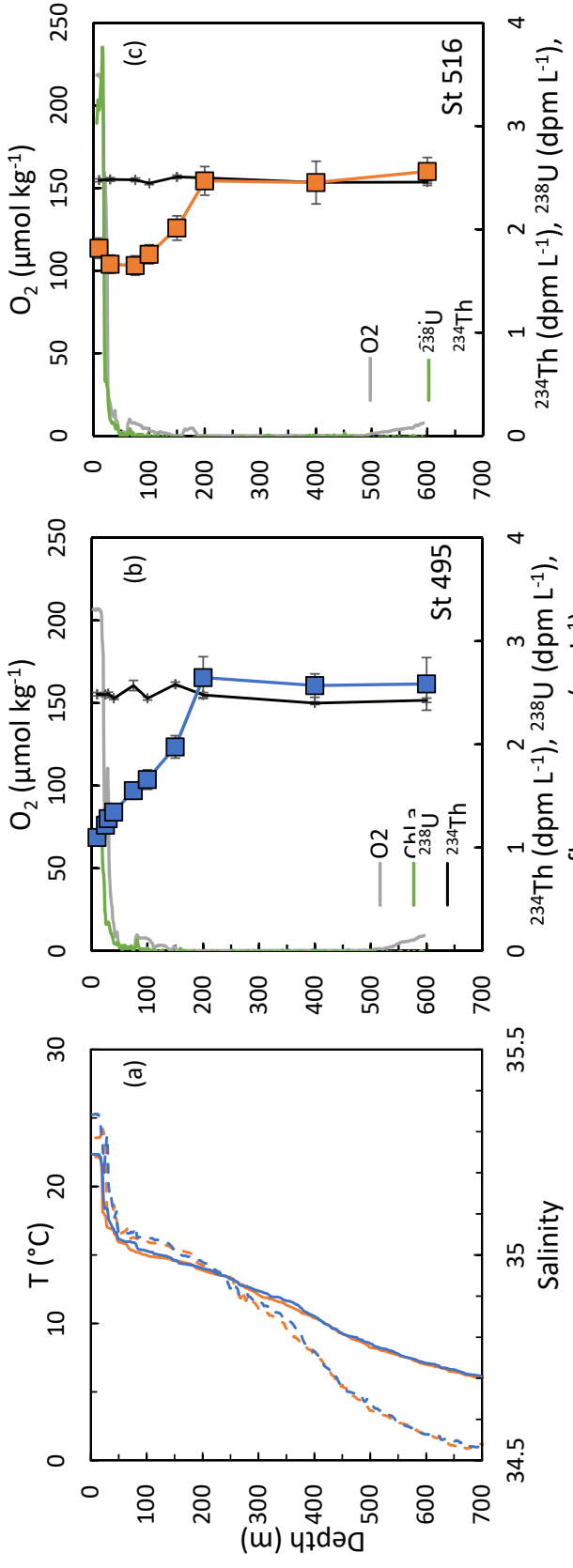

Figure 4

https://doi.org/10.5194/bg-2020-57
Preprint. Discussion started: 9 March 2020

Biogeosciences
Discussions
Open Access
EGU

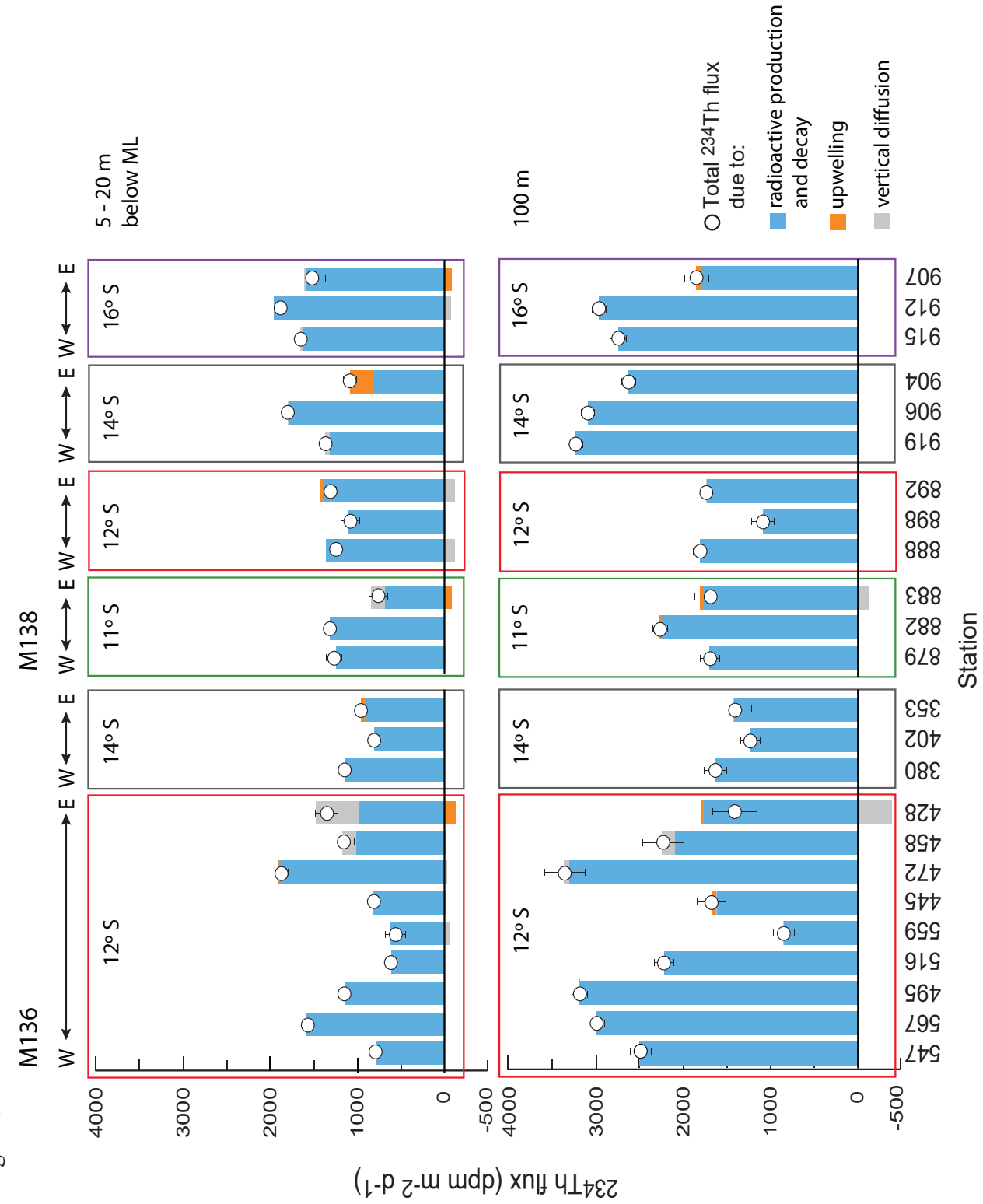

Figure 5

https://doi.org/10.5194/bg-2020-57
Preprint. Discussion started: 9 March 2020

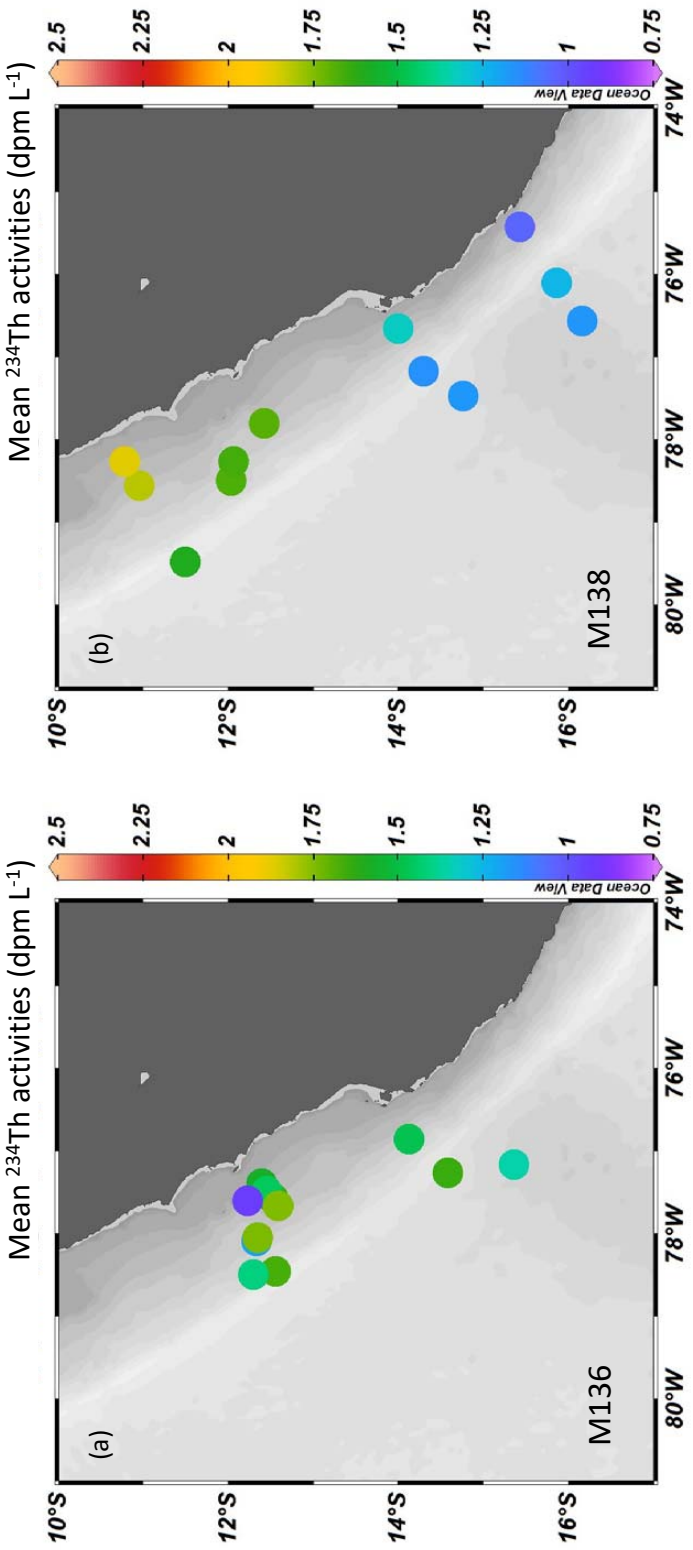

Figure 6